

Frequency combs based on magnon-skyrmion interaction in magnetic nanotubes

Tijjani Abdulrazak, Xuejuan Liu(刘雪娟), Zhejunyu Jin(金哲珺雨), Yunshan Cao(曹云姗), and Peng Yan(严鹏)
Citation: Chin. Phys. B, 2024, 33 (**8**): 087503. DOI: 10.1088/1674-1056/ad4ff5

What follows is a list of articles you may be interested in

Evolution of anomalous Hall effect in ferromagnetic Weyl semimetal $Nb_xZr_{1-x}Co_2Sn$

Bo-wen Chen(陈博文) and Bing Shen(沈冰)
Chin. Phys. B, 2024, 33 (**8**): 087501. DOI: 10.1088/1674-1056/ad4a3b

Critical behavior of quasi-two-dimensional ferromagnet $Cr_{1.04}Te_2$

Wei Niu(钮伟), Qin-Xin Song(宋沁心), Shi-Qi Chang(常世琦), Min Wang(王敏), Kui Yuan(袁奎), Jia-Cheng Gao(高嘉程), Shuo Wang(王硕), Zhen-Dong Wang(王振东), Kai-Fei Liu(刘凯斐), Ping Liu(刘萍), Yong-Bing Xu(徐永兵), Xiao-Qian Zhang(张晓倩), and Yong Pu(普勇)
Chin. Phys. B, 2024, 33 (**7**): 077506. DOI: 10.1088/1674-1056/ad4cd8

RKKY interaction in helical higher-order topological insulators

Sha Jin(金莎), Jian Li(李健), Qing-Xu Li(李清旭), and Jia-Ji Zhu(朱家骥)
Chin. Phys. B, 2024, 33 (**7**): 077503. DOI: 10.1088/1674-1056/ad3ef9

Relationship between disorder, magnetism and band topology in $Mn(Sb_{1-x}Bi_x)_2Te_4$ single crystals

Ming Xi(席明) and Hechang Lei(雷和畅)
Chin. Phys. B, 2024, 33 (**6**): 067503. DOI: 10.1088/1674-1056/ad3dd8

Magnetic and magnetocaloric effect of $Er_{20}Ho_{20}Dy_{20}Cu_{20}Ni_{20}$ high-entropy metallic glass

Shi-Lin Yu(于世霖), Lu Tian(田路), Jun-Feng Wang(王俊峰), Xin-Guo Zhao(赵新国), Da Li(李达), Zhao-Jun Mo(莫兆军), and Bing Li(李昺)
Chin. Phys. B, 2024, 33 (**5**): 057502. DOI: 10.1088/1674-1056/ad1a94

Frequency combs based on magnon–skyrmion interaction in magnetic nanotubes

Tijjani Abdulrazak[1,2,‡], Xuejuan Liu(刘雪娟)[1,3], Zhejunyu Jin(金哲珺雨)[1], Yunshan Cao(曹云姗)[1], and Peng Yan(严鹏)[1,†]

[1] *School of Physics and State Key Laboratory of Electronic Thin Films and Integrated Devices, University of Electronic Science and Technology of China, Chengdu* 610054, *China*
[2] *Department of Physics, Bayero University, Kano*-700006, *Nigeria*
[3] *School of Healthcare Technology, Chengdu Neusoft University, Chengdu* 611844, *China*

(Received 5 February 2024; revised manuscript received 9 May 2024; accepted manuscript online 24 May 2024)

Within the magnonics community, there has been a lot of interests in the magnon–skyrmion interaction. Magnons and skyrmions are two intriguing phenomena in condensed matter physics, and magnetic nanotubes have emerged as a suitable platform to study their complex interactions. We show that magnon frequency combs can be induced in magnetic nanotubes by three-wave mixing between the propagating magnons and skyrmion. This study enriches our fundamental comprehension of magnon–skyrmion interactions and holds promise for developing innovative spintronic devices and applications. This frequency comb tunability and unique spectral features offer a rich platform for exploring novel avenues in magnetic nanotechnology.

Keywords: ferromagnetic, magnetic field, magnon, Mumax3 software, skyrmion

PACS: 75.50.Gg, 71.35.Ji, 12.39.Dc, 75.30.Ds **DOI:** 10.1088/1674-1056/ad4ff5

1. Introduction

Over the past few decades, frequency combs have drawn attention from various scientific sectors. For instance, optical frequency combs greatly influence metrology, making frequency measurements more precise.[1–3] A spectrum with several discrete, uniformly spaced spectral lines creates a frequency comb.[4] Its application in optical systems utilizing a mode-locked laser's pulse train was first proposed,[5] and it was later made possible in microresonators by applying Kerr nonlinearity.[6] Applications requiring high-precision frequency metrology, such as the optical atomic clock, optical ruler, exoplanet search, and molecular spectra sampling, depend on the optical frequency comb's ability to convert electromagnetic waves at optical and microwave frequencies mutually.[2,7–9] Scientists are searching for alternate frequency comb generators due to the popularity of photonic frequency combs. Recently, phononic combs were achieved in tiny extensional mode resonators,[10] and theoretical predictions[11] were made through a three-wave mixing procedure. Magnonic systems have been found to exhibit a variety of exotic phenomena, including squeezed states, antibunching, Bose–Einstein condensation, and multi-particle entanglement.[12–18]

Interaction between these factors broadens the scope of conventional spintronics and magnonic systems as a viable contender for quantum computing and quantum information processing. Despite these similarities, the analogy of frequency combs within a magnonic system is less explored. Three- and four-magnon processes are magnetic media's most prominent nonlinear effects. The three-magnon process can produce a frequency comb, although this is typically not very strong because of the low dipolar interaction. The intense exchange force dominates the four-magnon contact, but the produced magnon spectrum is continuous in two and higher dimensions.[4] Thus, creation of frequency combs continues to be an intriguing and challenging subject. Recent research has shown that magnetic texturing can dramatically improve the nonlinear three-magnon interaction in magnetic systems.[19–21] Among the magnetic textures, magnetic skyrmions are a fascinating class that may be used in fundamental physics and spintronic devices. It has been demonstrated recently that nonlinear scattering of polarized magnons off the skyrmion in antiferromagnets can produce a terahertz (THz) magnon frequency comb.[4] However, how propagating magnons and skyrmions interact nonlinearly in magnetic nanotubes is unknown. It is still being determined whether the magnon–skyrmion interaction can produce the magnon frequency comb and how the strength of the three-wave mixing is influenced by the direction in which the incident magnons propagate.

In this work, we consider a ferromagnetic nanotube with an out-plane magnetic anisotropy, the Dzyalonshinskii–Moriya interaction (DMI), and we use micromagnetic simulations to study magnon–skyrmion interaction in magnetic nanotubes as a function of geometrical and magnetic parameters.

†Corresponding author. E-mail: yan@uestc.edu.cn
‡Corresponding author. E-mail: atijjani.phy@buk.edu.ng

© 2024 Chinese Physical Society and IOP Publishing Ltd

Since a cylindrical nanotube has no borders, it is an attractive curved system to nucleate and transport skyrmions due to the possibility of avoiding their annihilation at the system's border caused by the skyrmion Hall effect. The model shows a substantial critical microwave field, so single-tone driving cannot induce the magnon frequency comb. By utilizing a two-tone driving, we observe the emergence of MFC, originating from the three mixings between propagation magnon–skyrmion interactions. This research contributes to the fundamental understanding of magnon–skyrmion interactions through theoretical models and experimental validations. It paves the way for the development of innovative spintronic technologies.

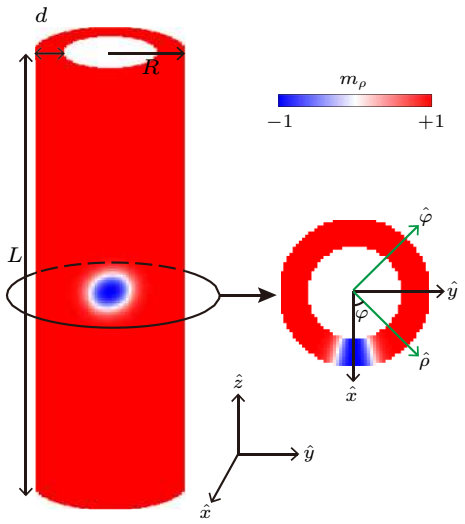


Fig. 1. Illustration of a Bloch-type skyrmion stabilized on a magnetic nanotube, with R and d representing the outer radius and thickness, respectively. The tube center is the origin, and the radial distances from the axial, azimuthal, and nanotube axes are represented by the values of $\hat{\rho}$, $\hat{\phi}$, and $\hat{z}$, respectively.

2. Model and numerical simulation procedure

We consider a magnetic nanotube with an outer radius $R = 50$ nm, thickness $d = 20$ nm, length $L = 600$ nm, and a cell size of 2 nm × 2 nm × 2 nm, as shown in Fig. 1. The exchange constant $A_{\rm ex} = 8.78$ pJ/m, saturation magnetization $M_{\rm s} = 2 \times 10^5$ A/m, bulk DMI parameter $D = 1$ mJ/m^2, easy-normal anisotropy constant $K_\rho = 2 \times 10^5$ J/m^3, and damping constant $\alpha = 0.001$ are taken for the FeGe material.[22] The open-source software Mumax3 package is the tool we employ for micromagnetic simulations.[23] The evolution of magnetization in magnetic systems can be studied numerically by solving the Landau–Lifshitz–Gilbert (LLG) equation

$$\frac{\partial \boldsymbol{m}}{\partial t} = -\gamma\mu_0 \boldsymbol{m} \times \boldsymbol{H}_{\rm eff} + \alpha \boldsymbol{m} \times \frac{\partial \boldsymbol{m}}{\partial t}, \tag{1}$$

where $\boldsymbol{m}$ is the unit vector of the magnetization, γ the gyromagnetic ratio, μ_0 the vacuum permeability, α the Gilbert damping, $\boldsymbol{H}_{\rm eff} = -\frac{1}{M_{\rm s}} \frac{\delta \varepsilon}{\delta \boldsymbol{m}}$ the effective field, and $\varepsilon = \varepsilon_{\rm ex} + \varepsilon_{\rm DMI} + \varepsilon_{\rm K} + \varepsilon_{\rm Dip}$ is the magnetic energy density, which includes the contributions from the exchange ($\varepsilon_{\rm ex}$), bulk Dzyaloshinskii–Moriya (DMI) ($\varepsilon_{\rm DMI}$), and anisotropy ($\varepsilon_{\rm K}$).

The energy density of the system reads

$$\varepsilon = A_{\rm ex}(\nabla \boldsymbol{m})^2 + D\boldsymbol{m} \cdot (\nabla \times \boldsymbol{m}) - K_\rho (\boldsymbol{m} \cdot \hat{\rho})^2, \tag{2}$$

where $A_{\rm ex}$ is the exchange constant, D is the bulk Dzyaloshinskii–Moriya (DMI) constant, and K_ρ is the anisotropy constant along $\hat{\rho}$.

We initially performed micromagnetic simulations to obtain stable skyrmion on the nanotube as shown in Fig. 1, by positioning the initial state at the center of the nanotube.

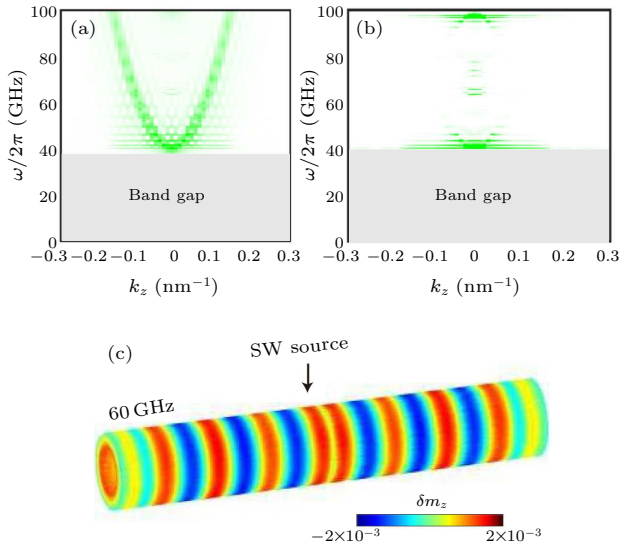


Fig. 2. (a) Magnon dispersion obtained by micromagnetic simulation without skyrmion. (b) Magnon dispersion relation with skyrmion. (c) A snapshot in time of the magnon profiles at excitation frequency 60 GHz.

3. Results and discussion

3.1. Magnon propagation in nanotubes

We first study magnon propagation in magnetic nanotubes before examining the interaction between magnons and skyrmion. We consider a uniform magnetization along the radial direction $m_0 = \hat{\rho}$ (without the skyrmion) as the ground state, since the anisotropic field ($\frac{2K_\rho}{M_{\rm s}} = 2.0$ T) is much larger than the demagnetization field ($\mu_0 M_{\rm s} = 0.25$ T). In the dynamical simulations, a Gilbert damping of $\alpha = 0.001$ is used to guarantee the magnon's long-distance propagation, and absorbing boundary conditions are chosen to prevent the tube ends' magnon reflection. To simulate the magnon dispersion, we apply a sinc-function microwave field $\boldsymbol{h}(t) = h_0 \sin[\omega_{\rm c}(t - t_0)]/[\omega_{\rm c}(t - t_0)]\hat{z}$ with $\mu_0 h_0 = 100$ mT, $\omega_{\rm c}/2\pi = 100$ GHz, and $t_0 = 1$ ns at the center section of the nanotube. The magnon dispersion relation acquired by the fast Fourier transform of δm_z is shown in Fig. 2(a). The dispersion relation exhibits a parabolic shape, and we observed a non-zero frequency when k_z approaching zero due to the band gap that comes from the anisotropy. In Fig. 2(a), we observe a band gap width

of 40.8 GHz as k_z approaching zero, while in Fig. 2(b), the presence of skyrmion decreases the band gap, introduces additional magnetic interaction which affects the dispersion of the magnons and also leads to the emergence of new modes as shown in Fig. 3(a). Figure 2(c) shows a snapshot in time of the magnon profile at the exciting frequency $\omega_b/2\pi = 60$ GHz (generating the incident magnon of wavelength ≈ 57.1 nm). One can see that magnons with opposite propagating directions have the same wavelength, indicating that no asymmetric magnon dispersion is induced by the curvature effect in nanotubes with the radial magnetization $m_\rho = 1$.

3.2. Magnon–skyrmion interaction in magnetic nanotube

In order to study the skyrmion's intrinsic magnon excitation spectrum in a magnetic nanotube, we apply a sinc-function field in the tube, $\boldsymbol{h}(t) = h_0 \sin[\omega_c(t-t_0)]/[\omega_c(t-t_0)]\hat{z}$ with $h_0 = 100$ mT and cutoff frequency $f_c = 100$ GHz. A fast Fourier transform (FFT) is performed for each cell in the magnetic field system to obtain the internal spectrum, which is then averaged over the entire tube. As illustrated in Fig. 3(a), four main frequencies of 6.5 GHz, 9.2 GHz, 34.1 GHz, and 40.6 GHz are identified, and a thorough analysis of the magnon modes of the skyrmion in magnetic nanotube is conducted. Only the 40.8 GHz mode is visible in the δm_z spectrum of the magnon dispersion when there is no skyrmion. Compared to the magnon–skyrmion interaction mode, the 40.6 GHz mode is a ferromagnetic resonance (FMR) mode.

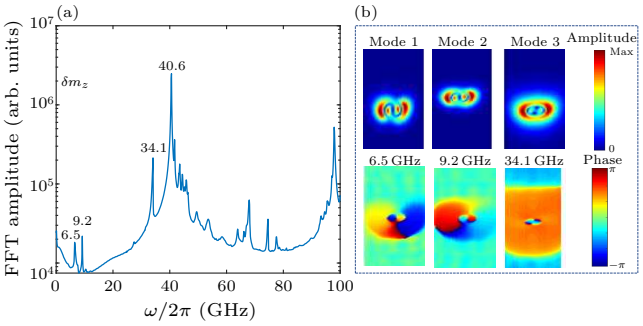


Fig. 3. (a) The internal spectrum of the magnetic nanotube with a skyrmion. (b) The magnon modes of skyrmion in a magnetic nanotube, with the first and second rows showing fast Fourier transform amplitude and phase of δm_z.

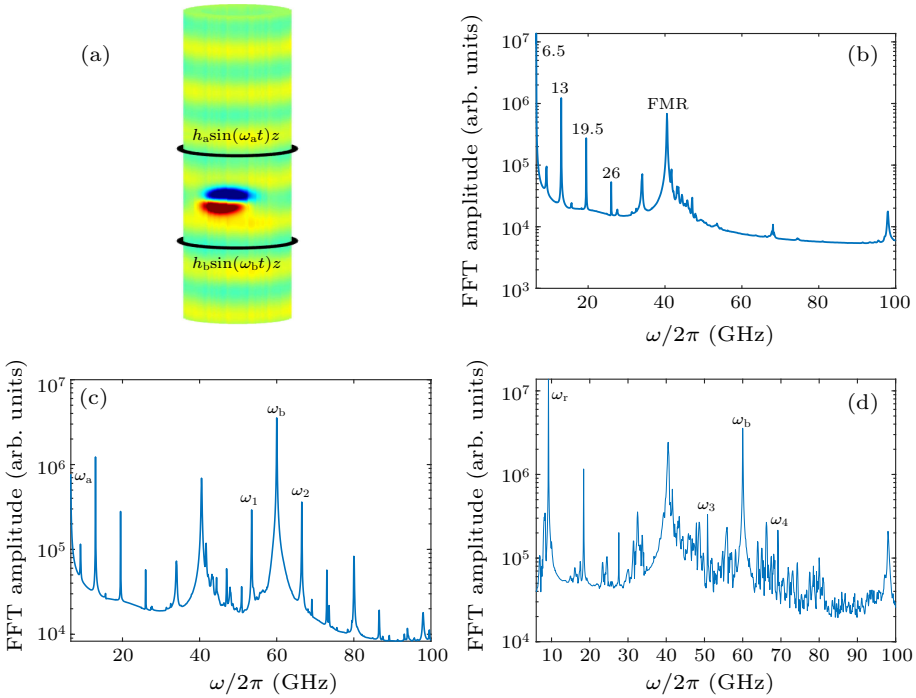


Fig. 4. (a) Snapshot of magnon–skyrmion interaction in magnetic nanotube hosting a Bloch-type skyrmion. The incident spin-waves and skyrmion gyrotropic are triggered by microwave fields $h(t) = h_b \sin(\omega_b t)\hat{z}$ and $h(t) = h_a \sin(\omega_a t)\hat{z}$, respectively, with black ring. (b) The detecting region's magnon spectrum in (a) for the exciting field $h_b = 100$ mT and $\omega_b = 60$ GHz of magnon is applied. (c) Magnon frequency combs in the nonlinear interaction between the magnon and skyrmion for skyrmion gyrotropic mode 1 ($\omega_a = 6.5$ GHz). (d) Magnon frequency combs in the nonlinear interaction between the magnon and skyrmion for skyrmion gyrotropic mode 2 ($\omega_r = 9.2$ GHz).

Mode 1, at 6.5 GHz, is a gyrotropic mode, where the resonance amplitude in δm_z of the outer and inner skyrmion is more significant in the magnetization zone. The inner skyrmion experiences phase changes that are opposite to those of the outer skyrmion, with the phase profile of the outer skyrmion's spatial distribution changing continuously from $-\pi$ to π. Mode 2, at 9.2 GHz, is a gyrotropic mode, where the resonance amplitude of the outer skyrmion is larger than that of the inner skyrmion. The inner skyrmion experiences phase changes opposite to those of the outer skyrmion, with

the phase profile of the outer skyrmion's spatial distribution changing continuously from $-\pi$ to π. Mode 3, at 34.1 GHz, is a breathing mode, where the resonance amplitude of the outer skyrmion is larger than that of the inner skyrmion. The inner skyrmion experiences phase changes opposite to those of the outer skyrmion, with the phase profile of the outer skyrmion's spatial distribution changing continuously from $-\pi$ to π. Additionally, through examining the skyrmion movement when subjected to sinusoidal microwave driving of 6.5 GHz, 9.2 GHz, and 34.1 GHz frequency modes, we identify mode 1 and mode 2 as counterclockwise gyrotropic modes and clockwise hybrid mode, respectively. A three-wave splitting mechanism can be used in ferromagnetic materials to ignite the skyrmion gyrotropic mode when the local intriguing field's amplitude reaches a specific threshold. The subsequent wave-mixing causes a magnon frequency comb.[4] This concept drives our usage of a linearly polarized microwave field $\boldsymbol{h}(t) = h_{\mathrm{a}}\sin(\omega_{\mathrm{a}}t)\hat{z}$ with $h_{\mathrm{a}} = 100$ mT and $\omega_{\mathrm{a}}/2\pi = 6.5$ GHz within a narrow circular region [black ring with $h_{\mathrm{a}}\sin(\omega_{\mathrm{a}}t)\hat{z}$ Fig. 4(a)] to trigger the magnon incident.

The magnon interacts with the skyrmion with the aim of generating a magnon frequency comb. However, the field amplitude was increased from 100 mT to 700 mT and we observed no signs of magnon frequency comb except for the incident magnon mode and its frequency-doubling signal as shown in Fig. 4(b) for 100 mT. To overcome this challenge, we introduced an additional micro-wave field $h(t) = h_{\mathrm{b}}\sin(\omega_{\mathrm{b}}t)\hat{z}$ with $h_{\mathrm{b}} = 100$ mT and $\omega_{\mathrm{b}}/2\pi = 60$ GHz within a narrow circular region [black ring with $h_{\mathrm{b}}\sin(\omega_{\mathrm{b}}t)\hat{z}$ in Fig. 4(a)] and the incident magnons interacted with the skyrmion mode. To ascertain whether the magnon frequency comb was generated, we analyzed the spectrum of magnon within the same region that excites the skyrmion by performing fast Fourier transform (FFT) of the magnetization in motion. Figure 4(c) displays the gigahertz region's emerging magnon frequency comb (MFC), where the comb's mode spacing is precisely equal to the skyrmion gyrotropic frequency.[24] Consequently, the incident magnon mode (ω_{b}) and the skyrmion gyrotropic mode 1 (ω_{a}) generate sum-frequency $\omega_2 = \omega_{\mathrm{b}} + \omega_{\mathrm{a}} = 66.5$ GHz and difference-frequency $\omega_2 = \omega_{\mathrm{b}} - \omega_{\mathrm{a}} = 53.5$ GHz. Figure 4(d) shows that the incident magnon mode (ω_{b}) and the skyrmion gyrotropic mode 2 (ω_{r}) generate sum-frequency $\omega_4 = \omega_{\mathrm{b}} + \omega_{\mathrm{r}} = 69.2$ GHz and difference-frequency $\omega_3 = \omega_{\mathrm{b}} - \omega_{\mathrm{r}} = 50.8$ GHz. In Figs. 4(c) and 4(d), we can obtain frequency combs for $\omega_{\mathrm{b}} \pm n\omega_{\mathrm{a}}$ and $\omega_{\mathrm{b}} \pm n\omega_{\mathrm{r}}$, with integer n. Recent studies have highlighted the intriguing magnetic properties of two-dimensional 1T-$CrTe_2$, and demonstrated that the Kitaev interaction, along with single-ion anisotropy and other off-diagonal exchanges, can account for the observed magnetic orientation in 1T-$CrTe_2$. That study sheds light on the complex magnetic behavior of 1T-$CrTe_2$, elucidating the underlying mechanisms that govern its magnetic properties and highlighting its potential in spintronic applications.[25,26]

4. Conclusion

In conclusion, we have uncovered an interplay between skyrmions and magnons in magnetic nanotubes, which leads to formation of magnonic frequency combs. It is found that exiting the gyrotropic skyrmion motion with a single-tone propagating magnon is difficult due to its huge threshold microwave field amplitude. Therefore, we introduce an additional low-frequency driving source to generate the magnon frequency comb. The spectral lines that are distinct and evenly spaced, which are typical of frequency combs, provide crucial information on the dynamic behavior of confined spin systems. We have demonstrated that the intricate coupling of magnons and skyrmions can form stable frequency combs, holding great promise for applications in spintronic devices. Furthermore, our results provide insight into developing and manipulating complicated spin textures, thus expanding our understanding of magnon–skyrmion interactions in constrained geometries. The controllable and engineered frequency combs in magnetic nanotubes create more opportunities for developing sophisticated spintronic technologies, such as spin wave-based computing and magnonic logic devices.

Acknowledgments

This project was supported by the National Key R&D Program China (Grant No. 2022YFA1402802) and the National Natural Science Foundation of China (Grant Nos. 12374103 and 12074057). Tijjani sincerely thanks every team member, especially Dr. Zhenyu Wang, for their invaluable contributions to the accomplishment of this project.

References

[1] Bellini M and Hänsch T W 2000 *Opt. Lett.* **14** 1049
[2] Fortier T and Baumann E 2019 *Commun. Phys.* **2** 153
[3] Jones D J, Diddams S A, Taubman M S, Cundiff S T, Ma L S and Hall J L 2000 *Opt. Lett.* **5** 308
[4] Wang Z, Yuan H Y, Cao Y, Li Z X, Duine R A and Yan P 2021 *Phys. Rev. Lett.* **127** 037202
[5] Udem T, Holzwarth R and Hänsch T W 2002 *Nature* **416** 233
[6] Del'Haye P, Schliesser A, Arcizet O, Wilken T, Holzwarth R and Kippenberg T J 2007 *Nature* **450** 1214
[7] Pasquazi A, Peccianti M, Razzari L, Moss D J, Coen S, Erkintalo M, Chembo Y K, Hansson T, Wabnitz S, Del'Haye P, Xue X, Weiner A M and Morandotti R 2018 *Phys. Rep.* **729** 81
[8] Suh M G, Yi X, Lai Y H, Leifer S, Grudinin I S, Vasisht G, Martin E C, Fitzgerald M P, Doppmann G and Wang J 2019 *Nat. Photon.* **13** 25
[9] Dutt A, Joshi C, Ji X, Cardenas J, Okawachi Y, Luke K, Gaeta A L and Lipson M 2018 *Sci. Adv.* **4** 1701858
[10] Ganesan A, Do C and Seshia A 2017 *Phys. Rev. Lett.* **118** 033903
[11] Cao L S, Qi D X, Peng R W, Wang M and Schmelcher P 2014 *Phys. Rev. Lett.* **112** 075505
[12] Nikuni T, Oshikawa M, Oosawa A and Tanaka H 2000 *Phys. Rev. Lett.* **84** 5868

[13] Zhao J, Bragas A V, Lockwood D J and Merlin R 2004 *Phys. Rev. Lett.* **93** 107203
[14] Bender S A, Duine R A and Tserkovnyak Y 2012 *Phys. Rev. Lett.* **108** 246601
[15] Flebus B, Bender S A, Tserkovnyak Y and Duine R A 2016 *Phys. Rev. Lett.* **116** 117201
[16] Kamra A, Thingstad E, Rastelli G, Duine R A, Brataas A, Belzig W and Sudbø A 2019 *Phys. Rev. B* **100** 174407
[17] Liu Z X, Xiong H and Wu Y 2019 *Phys. Rev. B* **100** 134421
[18] Yuan H Y and Duine R A 2020 *Phys. Rev. B* **102** 100402
[19] Wolz T, Stehli A, Schneider A, Boventer I, Macêdo R, Ustinov A V, Kläui M and Weides M 2020 *Commun. Phys.* **3** 3
[20] Lachance-Quirion D, Wolski S P, Tabuchi Y, Kono S, Usami K and Nakamura Y 2020 *Science* **367** 425
[21] Yuan H Y, Zheng S, Ficek Z, He Q Y and Yung M H 2020 *Phys. Rev. B* **101** 014419
[22] Wang W, Albert M, Beg M, Bisotti M A, Chernyshenko D, Cortés-Ortuño D Hawke I and Fangohr H 2015 *Phys. Rev. Lett.* **114** 087203
[23] Vansteenkiste A, Leliaert J, Dvornik M, Helsen M, Garcia-Sanchez F and Waeyenberge F B V 2014 *AIP Adv.* **4** 107133
[24] Liang X, Xia J, Zhang X C, Ezawa M, Tretiakov O A, Liu X X, Qiu L, Zhao G P and Zhou Y 2021 *Appl. Phys. Lett.* **119** 062403
[25] Huang C, Liu B, Jiang L, Pan Y, Fan J, Shi D, Ma C, Luo Q and Zhu Y 2023 *Phys. Rev. B* **108** 094433
[26] Zhu Y, Pan Y F, Ge L, Fan J Y, Shi D N, Ma C L, Hu J and Wu R Q 2023 *Phys. Rev. B* **108** 041401